CrossMark

Frost heave and frost heaving-induced pressure under various restraints and thermal gradients during the coupled thermal–hydro processes in freezing soil

Yukun Ji[1,2] · Guoqing Zhou[1] · Matthew R. Hall[2,3]

Abstract

Studies of frost heaving-induced pressure (FHIP) have been gaining increasing attention for applications using the freezing method to strengthen soils. This paper demonstrates a technique for measuring the FHIP when heaving is constrained. A series of freezing tests were conducted under various restrained stiffnesses and associated with a thermal gradient. The evolution of frost heave and the FHIP during coupled hydro–thermal interaction were examined. From this study, it was found that restraint prevents frost heave by impeding formation of the ice lens. A thermal gradient is a necessary condition for both water flow and frost heave, since pore water solidifies into ice and thus causes suction (negative pore water pressure) at the base of the ice lens. The pore structure and flow properties of freezing soil vary, since ice crystals progressively block the flow of water, whilst discontinuous ice lenses result in variation of water distributions. The increase of the FHIP appeared to cease when the ice pressure reached a maximum value, based on the microscopic analysis of equivalent water pressure. Moreover, the stable stage for the FHIP lagged behind the stabilization temperature. A macroscopic analysis of the different FHIPs under various different restraints was also carried out. It was found that increased restrained stiffness caused increased deformation and resulted in an increase of the observed FHIP. The coupled hydro–thermal behaviors analyzed in this study enable a better understanding of heat transfer and fluid flow in freezing granular media (soils).

Introduction

In recent decades, the freezing method has been widely applied in underground engineering due to its reliable performance for strengthening soil and groundwater cutoff, i.e., mining engineering, tunneling, and nuclear waste storage engineering. In freezing soil, frost heave is a phenomenon which couples heat and mass transfer (Harlan 1973; Lai et al. 2014;

✉ Guoqing Zhou
gdue.zhou@gmail.com

1 State Key Laboratory for Geomechanics and Deep Underground Engineering, China University of Mining and Technology, Xuzhou 221116, Jiangsu, China

2 GeoEnergy Research Centre, Faculty of Engineering, University of Nottingham, Nottingham NG7 2RD, UK

3 British Geological Survey, Environmental Science Centre, Nottingham, Keyworth NG12 5GG, UK

O'Neill and Miller 1985; Taylor and Luthin 1978; Zhou and Zhou 2012) and is attributable mostly to the water that flows to the latest ice lens and freezes in the form of ice (Konrad and Morgenstern 1982; Nixon 1991; Wu et al. 2017). Due to the restraining effect of the engineering structure on frost heave, the FHIP occurs after the deformation of the structure (Ji et al. 2018). Furthermore, the FHIP acting on the engineering structure is directly responsible for flaking and cracking in the supported structure, and will cause some kind of potential geotechnical hazards in cold regions, such as water-leaking, hanging-ice and overbend deformation (Cheng and Li 2003; Lai et al. 2000; Palmer and Williams 2003).

So far, many research studies have been performed on the effect of the thermal gradient on frost heave (Gilpin 1979; Gilpin 1980; Konrad and Morgenstern 1982; Konrad 1994; Lai et al. 2014; Oliphant et al. 1983), and on the effect of constant applied pressure on frost heave (Bronfenbrener and Bronfenbrener 2010; Hopke 1980; Sheng et al. 1995a; Sheng et al. 1995b; Xia 2005; Zhang et al. 2017). These studies have found that the thermal gradient causes a suction gradient that

induces capillary water flow. The adsorbed water film (at a lower temperature) has lower free energy, thus water can then be sucked up from the warm portion to feed the latest ice lens, which is oriented perpendicular to the direction of water and heat flow. Additionally, the thermal gradient has a great effect on both the frost penetration and the frozen fringe thickness (water flow path). As for the effect of constant external pressure, it can be found that constant external pressure prevents frost heave by impeding formation of the ice lens, thickening the frozen fringe, and causing the decrease of the segregation temperature. Moreover, the water pressure which appears in suction at the bottom of the ice lens is also affected by the external pressure. Mechanistic frost heave models, with an applied constant pressure, are well established. Sheng et al. (Sheng et al. 2013) reported a discrete ice lens method to predict frost heave by including overburden effect on ice lensing and frozen fringe. Lai et al. (Lai et al. 2014) put forward a mechanistic frost heave model considering the thermal–hydro–mechanical processes, which provides an accurate prediction of frost heave with respect to overburden pressure. Many studies on frost heave are conducted with respect to constant applied pressure; however, the interaction between frost heave and the FHIP derived from the restrained structure is more common. A typical profile of artificial freezing engineering shows that the varying restrained stiffness of the shaft lining will cause different results for frost heave and the FHIP during freezing (Fig. 1). Moreover, the field measurement of the FHIP on the shaft lining shows that the FHIP in deep alluvium is about twice as large as the initial earth pressure (Wang et al. 2009), and is highly influenced by factors such as soil types, freezing condition, properties of support material, and so on (Ma and Cheng 2007). The field research also pointed out that the elastic modulus of the shaft lining has a great influence on the FHIP, when the elastic modulus of the

concrete increases from 360 MPa to 36000 MPa during the hardening process. The FHIP grows from 0.64 MPa to 5.41 MPa; approximately 9 times as large as the initial FHIP (Rong 2006). However, the analysis of the difference in FHIP under various different restrained structures has not previously been addressed in literature.

Restraint of the supported structure, and thermal gradient, both have a significant effect on the FHIP during frost heaving. There is an urgent need to investigate the FHIP under various restrained stiffnesses. In this paper, a one-dimensional FHIP testing apparatus was developed to perform the freezing tests under various restrained stiffnesses and thermal gradients. From the experimental results, the evolution of frost heave, the FHIP, and the hydro–thermal behavior during freezing are examined and discussed. Additionally, an analysis for the difference in the FHIP under various restrained stiffness is presented under a given thermal gradient.

Testing methodology

Soil properties and sample preparation

Xuzhou (China) silty clay was used to prepare the soil samples with a dry unit weight of 1.6g/cm^3, whilst the soil samples were vacuum saturated (73mmHg) for 24 hours until a saturation degree > 0.98 and an ultimate water content of 24% were achieved. Xuzhou silty clay has a clay fraction of 10% and a silt fraction of 86.5%. It has a liquid limit of 28.92% and plastic limit of 16.23%. A Plexiglas cube was used as the soil sample vessel with inner dimensions of 100mm × 100mm × 180mm, and petroleum jelly was used to lubricate and reduce the friction between the soil and vessel wall.

Fig. 1 Schematic of artificial freezing engineering and frost heave under restrained conditions
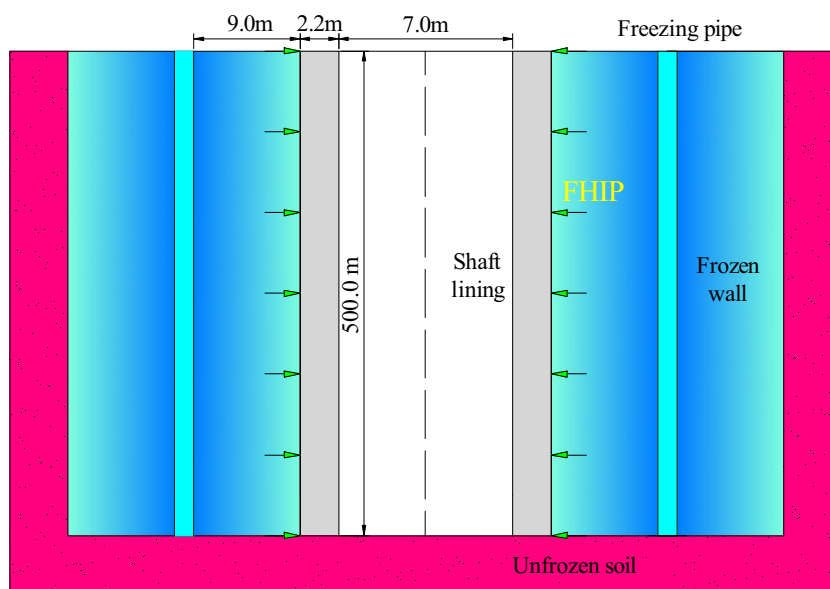
Testing apparatus and the procedures

For the one-dimensional FHIP testing apparatus, it is apparent that an elastic restraint is employed at the top of the soil column (Fig. 2). It should be noted that the elastic restraint is deformed with frost heave, resulting in the FHIP at the soil–restraint interface. The FHIP under the elastic restraint can be seen as a product of frost heave and restrained stiffness.

In order to eliminate errors caused by the ambient temperature, the experimental tests were carried out in a cold room maintained at a constant temperature of 2 $^{\circ}$C. Before freezing, identical initial thermal conditions were applied for all specimens, and the specific FHIP testing procedures of the freezing soils were conducted using the following four steps:

Step 1 Mount the sample. Firstly, the saturated specimens were poured into the Plexiglas cube. Secondly, the specimens were placed on the pedestal of the FHIP apparatus. Thirdly, the cold end and vertical elastic restraint were installed on the top of the specimens. A displacement sensor (type: YHD-50) with a range of 50mm and a linearity of ±2.5% was employed to measure the vertical displacement at the top of the specimen. The FHIP measurements under the rigid constraint were measured by a load sensor (type: H2F-C2-0.5t-4T6) with a precision of 0.03% and a range of 5.0t when the rigid restraint is applied. The stiffness of the load sensor is about 1221.7kPa/mm measured by the Servo Press. In addition,19 thermal resistors embedded in the specimen (type: MF5E-2.202F) measured the temperature along the

specimen, spaced at 10mm intervals. Finally, the mineral wool surrounding the Plexiglas cube was applied as insulation to approximate a one-dimensional thermal gradient.

Step 2 A thermostatic process. The water supply tube was turned off. Both warm and cold end were controlled at a constant temperature of 10 $^{\circ}$C until a thermostatic state is reached. The temperature was kept uniform longitudinally. The cryostats were applied to control the glycol mixture temperature ranging from −40 $^{\circ}$C to 90 $^{\circ}$C with a precision of ±0.05°C.

Step 3 Open system freezing. The water supply tube was switched on. The temperature of the warm end of the specimens was maintained at 10 $^{\circ}$C during the testing time, whilst the freezing temperature was set at the top of the specimens, and freezing progressed downward from the top of the specimen to the bottom.

Step 4 Data logging. Data Taker 800 and 515 were used to collect the temperature at different positions of the specimens, and to collect the displacement of frost heave. The installed sensors were set to take measurements at 1-minute intervals. The observed FHIP under various restrained stiffness values was the product of frost heave and the restrained stiffness.

After finishing the experimental tests, the soil columns were sliced into several soil columns of 1cm height, and the drying method was employed to measure the distribution of water content associated with the thermostat drying box DHG-9053A.
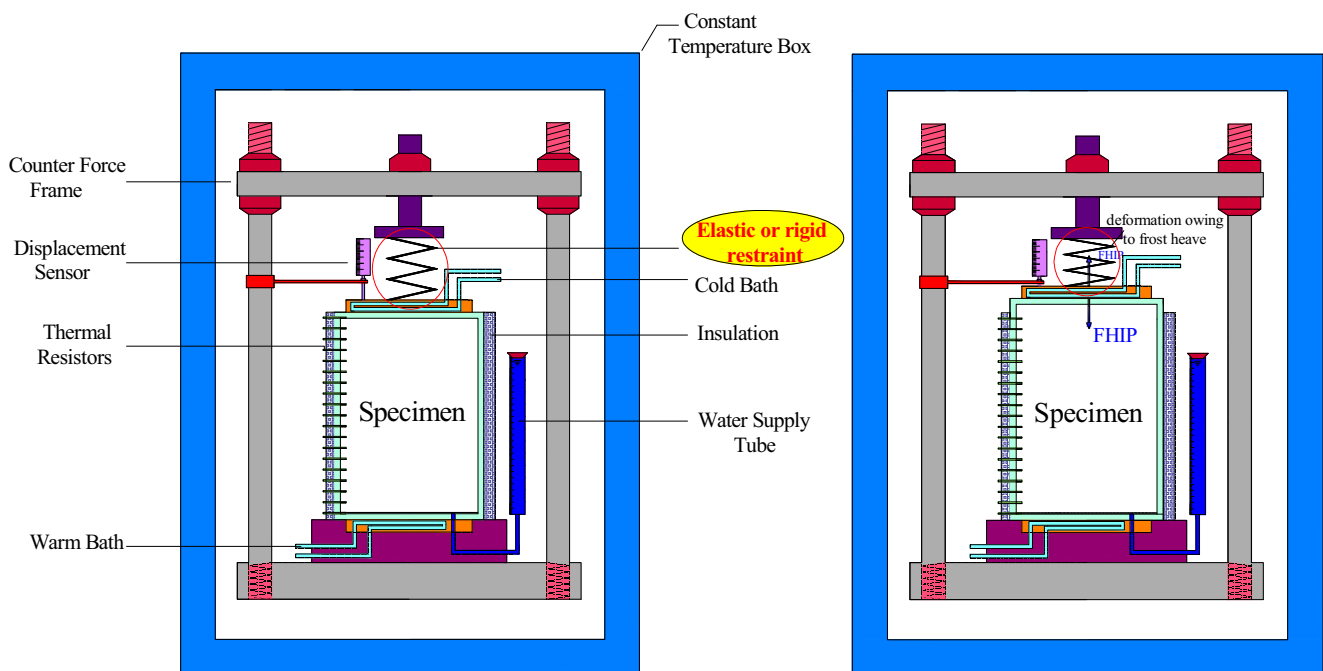
Fig. 2 One-dimensional FHIP testing apparatus: **a** before the appearance of frost heave; **b** after the appearance of frost heave

Testing scheme

The specimens were poured into the Plexiglas cube, and subjected to the restraints with stiffness values of 0.26, 11.06, 14.62, 21.36, or 28.02 kPa/mm (the restrained stiffness values were tested by the Serve Press). The testing scheme of the FHIP under various restrained stiffness values and subfreezing temperatures at the top of the tested samples is summarized in Table 1.

Results

Analysis of frost heave during freezing

The patterns of frost heave show a similar trend to one another (Fig. 3a). The development of frost heave can be generally distinguished into four stages. During the first 240 minutes, termed the *thermostatic stage* (I), no heave was observed. After 240 minutes, the first onset of freezing appeared. Frost heave grew rapidly with the penetration of the frost front, due to external water flowing into the frost front. This is identified as the *rapid development stage* (II). Subsequently, the *transitional development stage* (III) began 1300 minutes later; the frost front kept stationary within the specimens, and the rate of heave progression slowed down. Finally, the *stable stage* (IV) started (treated as the testing phase) after 2100 minutes; the heave rate gradually approached nearly zero. Moreover, frost heave decreased 60.7% from 10.97 mm to 4.31 mm, when the restrained stiffness increased from 0.00 kPa/mm to 21.36 kPa/mm under a given cold end temperature of -20 °C (Fig. 3a). This is because with the increase of the restrained stiffness, the formation of the ice lenses becomes more difficult, and thus causes an inhibiting effect for water flow from the unfrozen zone to the latest ice lens.

The ultimate results of frost heave under various restrained stiffness values and thermal gradients are demonstrated in Fig. 3b. Frost heave decreased as restrained stiffness increased under an identical cold end temperature. Additionally, it can be found that the decreasing cold end temperature increased frost heave. The frost heave increased 132.2% from 3.81 mm to 8.86 mm, when the cold end temperature decreased from −15 °C to −30 °C under a given restrained stiffness of 11.06 kPa/mm. In fact, the thermal gradient provides a pressure gradient which leads to water flow. An increase in the thermal gradient will facilitate the capillary flow of water in granular material.

### Relationship between frost heave rate and thermal gradient

A film of unfrozen water still exists during freezing in the soil pores. The adsorbed water film near the soil particles has a lower free energy at a lower negative temperature. A thermal gradient thus causes a gradient in the water potential, and water can then be sucked up from the warm portion to replace the water loss at the ice particle.

Different environmental scenarios will cause different results of frost heave velocity and thermal gradient. This section focuses on discussing the relationship between heave velocity and the thermal gradient. Because of the patterns of frost heave velocity, which present a similar trend, an environment scenario is selected as a representative when the freezing soil is under a restrained stiffness of 11.06 kPa/mm (constant cold end temperature of −20 °C). The thermal gradient (grad t= $(t_c - t_f)/H_p$) refers to the thermal gradient in the frozen zone, where t_c is the cold end temperature, t_f is the freezing temperature at the freezing front, and H_p denotes the depth of frozen zone. The tendency of heave velocity is highly consistent with the variation tendency of thermal gradient (Fig. 4), which illustrates that thermal gradient is the major factor to dominate frost heave.

Table 1 Testing scheme of the FHIP under various conditions

ID	T_w/°C	T_c/°C	Constrained boundary	K_1/kPa·mm^{-1}	ID	T_w/°C	T_c/°C	Constrained boundary	K_1/kPa·mm^{-1}
#1	10	−15	Free boundary	0	#11	10	−25	Free boundary	0
#2			Elastic restraint	0.26	#12			Elastic restraint	11.06
#3				11.06	#13				21.36
#4				21.36	#14				28.02
#5			Rigid restraint	∞	#15			Rigid restraint	∞
#6	10	−20	Free boundary	0	#16	10	−30	Free boundary	0
#7			Elastic restraint	11.06	#17			Elastic restraint	11.06
#8				14.62	#18				21.36
#9				21.36	#19				28.02
#10			Rigid restraint	∞	#20			Rigid restraint	∞

T_c and T_w are the temperatures at the top and bottom ends of the specimens, respectively; K_1 is the restrained stiffness applied on the specimens during freezing.
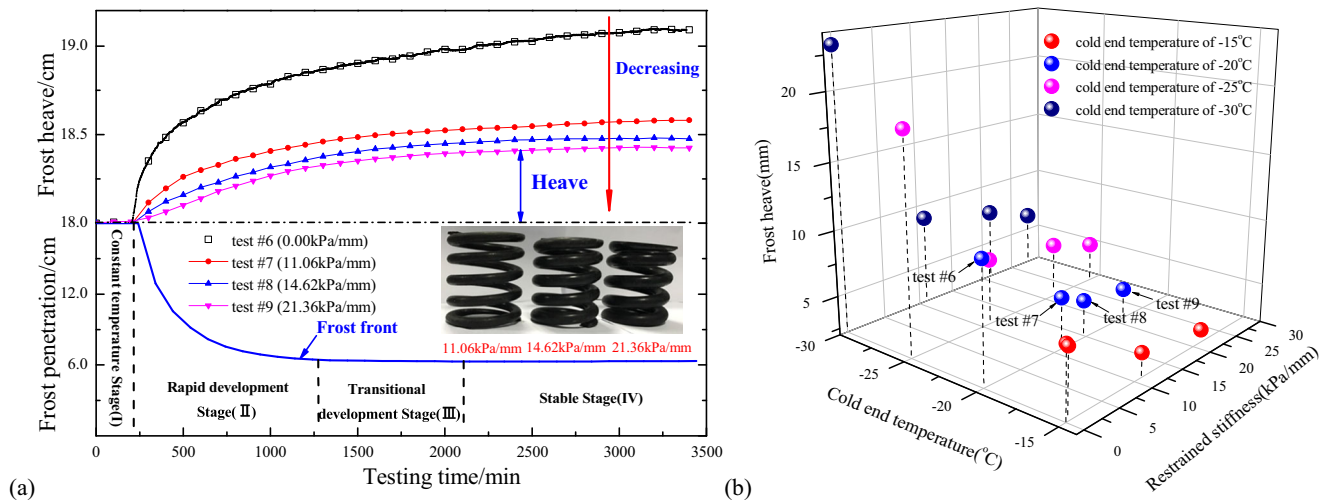
Fig. 3 Results of frost heave: **a** frost heave under different restrained stiffness values (constant cold end temperature of −20 °C); **b** frost heave under various restrained stiffness values and cold end temperatures

Water migration and distribution in freezing soil

Frost heave is highly dependent on the water migration in freezing soil. When the advancing frost front penetrates into the soil column, a water potential gradient develops as the temperature gradient increases. Negative water pressure (suction) occurs when the pore water solidifies into ice, and thus facilitates water migration from the unfrozen zone to feed the growth of the ice. Fig. 5 demonstrate a close look at the frozen fringe where phase transition occurs. According to the well-established Clausius–Clapeyron equation, water pressure P decreases as the temperature decreases under a specific ice pressure. Therefore, the pressure gradient is generated by the thermal gradient in partially frozen granular media (soil). As a result, there is a tendency for pore water to migrate from the warm side to the cold side, resulting in accumulation of pore ice and frost heave.

The distribution of water content (equivalent to unfrozen water and ice content) under different restraints and thermal gradients are provided in Fig. 6 for verification and investigation of frost heave under different environmental conditions. It can easily be seen that the maximum water content is found near the frost front (Fig. 6). As the restrained stiffness values increased, water content in the frozen zone decreased, since the suction at the warm side of ice lens decreases with increasing external pressure in the soil (Konrad and Morgenstern 1982). The results correspond to the analysis of frost heave under the restraint outlined in section "Analysis of frost heave during freezing". Furthermore, a new ice lens will emerge in the frozen fringe when the disjoining pressure at a certain place exceeds the sum of the external pressure and the critical pressure of soil strength. With the increase of restraint, the formation and growth of an ice lens becomes more difficult,

Fig. 4 Variation of frost heave velocity and thermal gradient under the restrained of 11.06 kPa/mm (constant cold temperature of −20 °C)
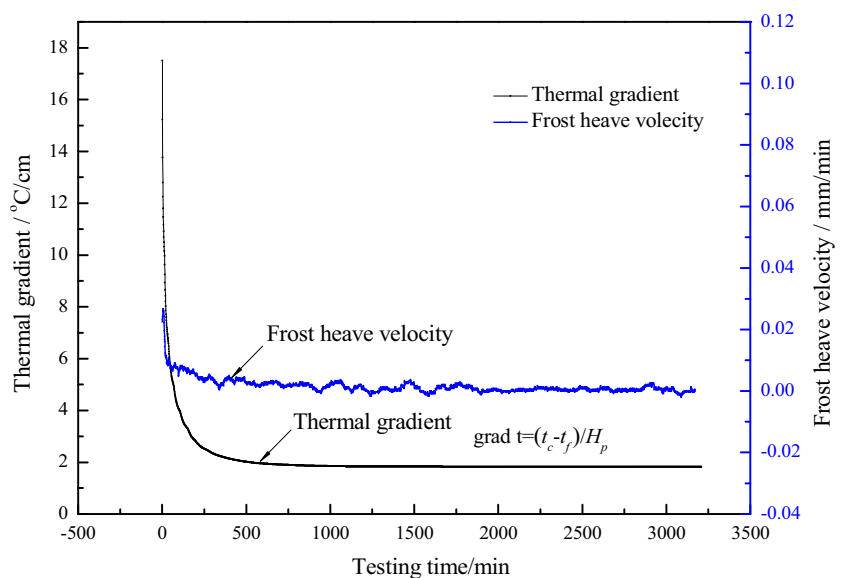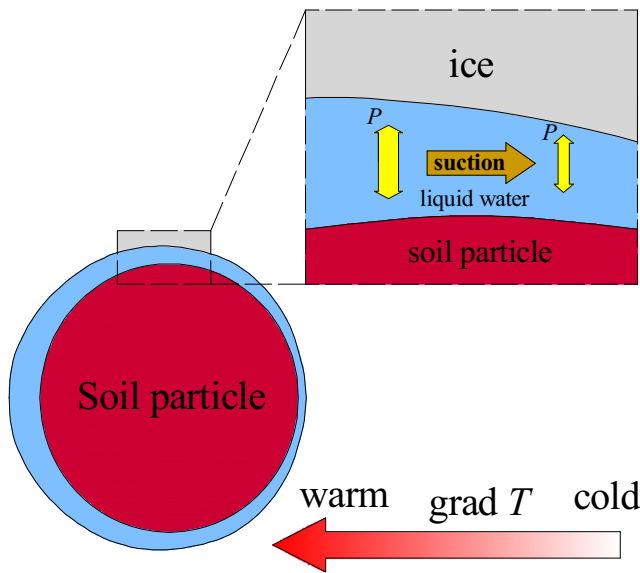
Fig. 5 Schematic of suction mechanism during freezing

thus causes an inhibiting effect for external water flows to the active ice lens. The lower position of the maximum water content caused by the lower cold end temperature is shown in Fig. 6b. Additionally, the water content near the frost front increases (and inversely with cold end temperature). Actually, lower cold end temperature accelerates the phase transition of pore water. The phase transition-induced negative pressure will drive water migration. The result demonstrates that the thermal gradient (suction gradient) dominates the movement of pore water, and it also confirms the relationship between frost heave and the thermal gradient outlined in section "Relationship between frost heave rate and thermal gradient". Furthermore, recent studies indicate that an increase in the thermal gradient results in the decrease of the frozen fringe thickness, making it more favorable for water flow (Sheng et al. 2013; Xia 2005).

In the frozen zone, the distribution of the water content was oscillatory due to the discrete ice lenses (Fig. 6a and b). The accumulation of the ice particles results in the formation of the horizontal ice lens, which is oriented perpendicular to the direction of water and heat flow. The warm end of the ice lens divides the soil column into two different hydraulic zones, i.e., the passive zone (frozen zone) and the active zone (which includes the unfrozen zone and the frozen fringe). The passive zone is mainly governed by heat conduction, while for the active zone, it is a coupled process of heat and mass transfer. After the formation of the second ice lens, the new ice lens will block the water migration to the previously growing ice lens. As shown in Fig. 6(a), several ice lenses will ultimately emerge until the warmest ice lens emerges. External water migrates into the frost front and feeds the growth of the warmest ice lens, and the thickest ice lens (maximum water content) will be found near the frost front. It can be illustrated that the soil-free ice lens is layered and discontinuously distributed (Fig. 6a) in the frozen zone up the frozen fringe.

In addition, the unsaturated phenomena in the unfrozen zone is explored. The water content in the unfrozen zone was lower than the initial saturated water content, even though the freezing test was conducted under the free boundary (Fig. 6a and b). The suction gradient induced by the temperature gradient at the ice–water interface will suck water to feed the accumulation of the ice particles. Konrad (Konrad 1994) stated that the suction increases linearly with decreasing temperature at a rate of 1250 kPa/°C based on the Clausius–Clapeyron equation. It can be concluded that a significant level of suction is generated at the ice–water interface. Xia (Xia 2005) conducted a series of experiments of frost heave, and reported that the negative water pressure not only provides the suction for
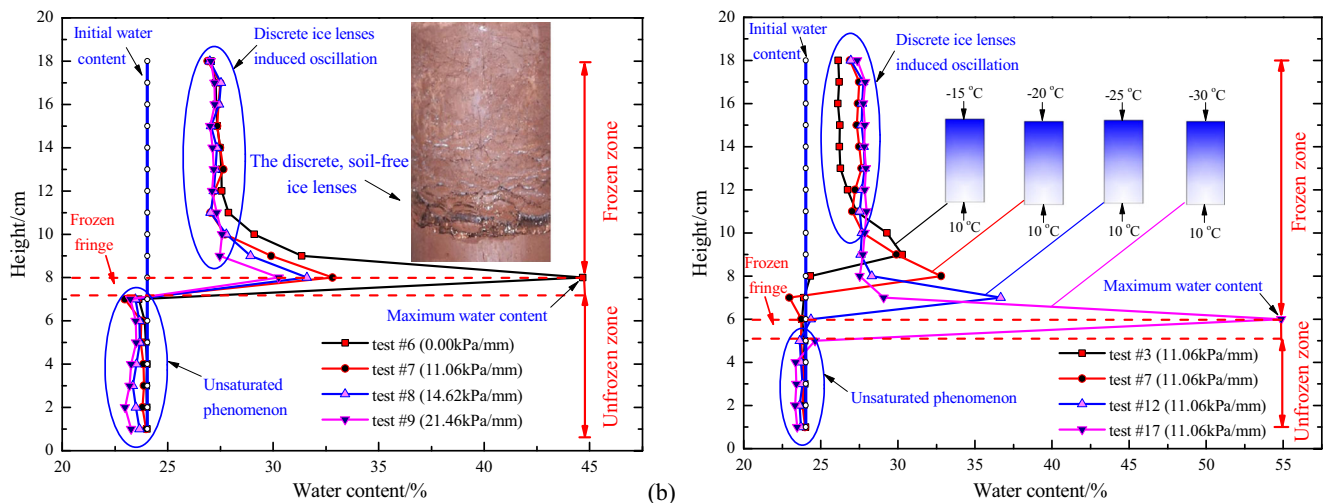

Fig. 6 Results of water content: a distribution of total water content under different restrained stiffness values (constant cold end temperature of −20 °C); b distribution of total water content under various cold end temperatures (constant restrained stiffness of 11.06 kPa/mm)

water to flow, but also results in the reduction of water content in unfrozen soil. In the unsaturated zone, Zhang et al. (Zhang et al. 2016) pointed out that ice formation may also be related to vapor migration, contributing the increased water content in freezing soil. The ice phase acts as a sink term, maintaining a density gradient and facilitating the vapor transfer. According to Fick's law, the migration velocity of vapor is related to the temperature gradient. Therefore, the suction effect and the temperature gradient might be the cause of unsaturated phenomena, since they will change pore structure of the soil column and induce water flow from the unfrozen zone to the ice lens.

The FHIP and maximum FHIP during freezing

The FHIP under elastic restraint is the product of frost heave and restrained stiffness. The FHIP under the rigid restraint is measured by the load sensor, with the maximum value taken as the ultimate value for the FHIP. The FHIP tested in this study are shown in Fig. 7(a) and (b), and the experimental data is presented in Table 2. It should be noted that for demonstration purposes, the restrained stiffness of the rigid restraint (∞) shown in abscissa is replaced by a restraint with stiffness of 200 kPa/mm (Fig. 7b).

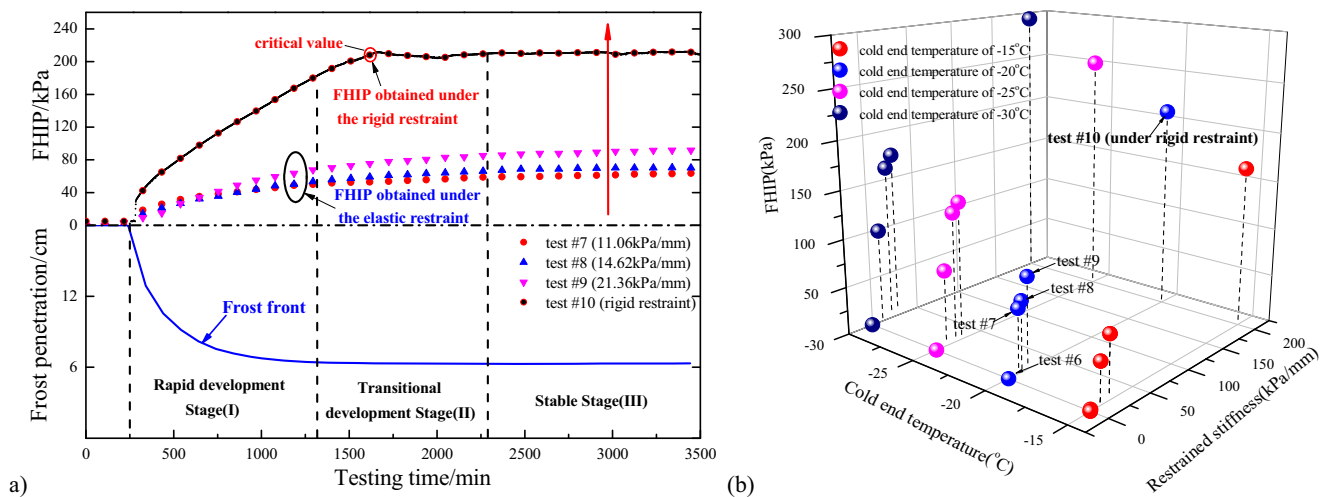The development of the FHIP under various restrained stiffness values associated with a constant cold end temperature of −20 °C are demonstrated in Fig. 7(a). It can be seen that the development of the FHIP (test #7, #8, and #9) during freezing can be divided into three stages, i.e., the *rapid development stage* (I), the *transitional stage* (II), and the *stable stage* (III). When the specimen was subjected to the sub-freezing temperatures from the top, the frost front advanced from the top down and the FHIP increased rapidly in stage I. The increasing rate of the FHIP decreased gradually after 1300 minutes in the transitional

Table 2 Results of frost heave and the FHIP under different restrained stiffness associated with cold end temperatures

ID	K_1 (kPa/mm)	Frost heave (mm)	Frost heaving ratio (%)	FHIP (kPa)
#1	0.00	7.22	6.95	0.0
#2	0.26	7.01	6.75	1.8
#3	11.06	3.81	3.67	42.1
#4	21.36	2.96	2.85	63.2
#5	∞	0.00	0.00	166.5
#6	0.00	10.97	9.40	0.0
#7	11.06	5.88	5.04	65.0
#8	14.62	4.86	4.17	71.1
#9	21.36	4.31	3.69	92.1
#10	∞	0.00	0.00	211.1
#11	0.00	18.29	14.89	0.0
#12	11.06	7.07	5.75	78.2
#13	21.36	6.24	5.08	133.3
#14	28.02	5.08	4.14	142.3
#15	∞	0.00	0.00	252.4
#16	0.00	23.12	18.07	0.0
#17	11.06	8.86	6.92	98.0
#18	21.36	7.57	5.92	161.7
#19	28.02	6.19	4.84	173.4
#20	∞	0.00	0.00	292.9

stage II. When the stable stage III began after 2100 minutes (treated as the testing phase), the growth rate of the FHIP gradually decreased close to zero.

The effect of cold end temperature on FHIP can be found in Fig. 7(b). The FHIP increased 132.8% from 42.1 kPa to 98.0 kPa, when the cold end temperature decreased from −15 °C to −30 °C under a given restrained stiffness of 11.06 kPa/mm. The increased thermal gradient

Fig. 7 Results of the FHIP: **a** the FHIP under different restrained stiffness values (constant cold end temperature of −20 °C); **b** the FHIP under various restrained stiffness values and cold end temperatures

is more favorable for water flow, resulting in an increase in frost heave and the FHIP (Konrad and Morgenstern 1982; Sheng et al. 2013). As for the effect of restraint, a contrary trend to the frost heave outlined in the section "Analysis of frost heave during freezing" above was observed, where the FHIP increased as the restrained stiffness increased (at a constant cold end temperature). The FHIP increased 41.1% from 65.0 kPa to 92.1 kPa, when the restrained stiffness increased from 11.06 kPa/mm to 21.36 kPa/mm under a given cold end temperature of −20 °C (Fig. 7a). To date, there are no literature reports to suggest a reason for this difference in the FHIP under various restraints. Further research to unravel what causes this will enable a better understanding of the characterized behavior of the FHIP under various restraints.

Perhaps more interestingly, the FHIP (test #10) under rigid restraint showed a different trend compared to the FHIP obtained under the elastic restraint. A small decrease of the FHIP occurred after the FHIP peaked at the critical value (*maximum heaving pressure*). In order to explain this significant phenomenon, some basic theories are presented below.

Zhou and Zhou (Zhou and Zhou 2012) adopted Gilpin's theory (Gilpin 1980) and defined a new concept of equivalent water pressure:

$$P = P_0 + P_{Lh} - P_{atm} - \frac{g(d)}{v_w} \tag{1}$$

where P_{Lh} is the disjoining pressure at the ice-water interface, $g(\cdot)$ is the effect of the solid surface, d is the thickness of the liquid layer, and v_w is specific volume of the liquid. The reference pressure P_0 in Gilpin's theory applied for the frozen zone is 1 atm, whilst for the unfrozen zone the reference pressure is equal to the local bulk water pressure. $P_{atm} = 1$ atm was chosen for both the unfrozen zone and the frozen zone. By substitution of $g(d) = -\Delta v P_{Lh} - v_i \sigma_{iw} \bar{K} - Lt/t_a$ into Eq. (1), the equivalent water pressure at the ice-water interface can be obtained by the following equation:

$$P = \frac{v_i}{v_w}\left(P_{Lh} + \sigma_{iw}\bar{K}\right) + \frac{Lt}{t_a v_w} = \frac{v_i}{v_w}P_e + \frac{Lt}{t_a v_w} \tag{2}$$

where v_i is the specific volume of the ice, σ_{iw} is the interfacial tension, $\bar{K}$ is the mean curvature of the ice-water interface, L is the latent heat, t is the temperature, $t_a = 273.15$K, and P_e is the ice pressure which equals to the overburden pressure. The second equality presented in Eq. (2) is the result when the Laplace equation is employed and a quasi-static process is regarded for the ice lens growth.

The water pressure at the ice–water interface provides a negative pressure as a result of the negative temperature t, causing suction and potential for capillary water to flow. Suction at the ice–water interface can be simplified as follows:

$$P = P_e + \frac{Lt}{t_a v_w} \tag{3}$$

Eq. (3) is not a complete description of the equivalent water pressure and neglects a term $(v_i/v_w - 1)P_e$, which is very small since $v_i \approx v_w$.

Furthermore, Worster and Wettlaufer (Worster and Wettlaufer 1999) showed that pressure drops occur in pre-melted films between ice and particles, causing a large resistance to water flow. Accordingly, the definition of equivalent water pressure could be improved by considering the effect of pre-melted films at the ice lens front. Style and Peppin (Style and Peppin 2012) deduced and defined a new concept of water pressure at the ice–water interface based on the force balance with a pressure, p in the film. A similar method is applied to determine the new equivalent water pressure at the ice–water interface, as shown in Eq. (4):

$$P - P_n = \mathbf{z} \cdot \frac{1}{A_1} \int_{A_2} (p - P_n)\mathbf{n}dA \tag{4}$$

where P_n is new definition of water pressure at the ice–water interface, p is the pressure in the thin pre-melted film, $\mathbf{z}$ is the unit vector in the z direction, $\mathbf{n}$ denotes the unit vertical normal to the ice–water interface, A_1 represents the ice lens area of the cross section, and A_2 is the underlying area at the ice–water interface.

From Eq. (4), it can be found that the film thickness between the overlying ice and porous medium will diverge into the 'bulk' pore fluid if $p \to P_n$. Assuming the fluid film freezes onto ice lens at a constant rate V, the expression $p - P_n = Vg(x, t)$ can be obtained based on the general linearity lubrication theory, where $g(x, t)$ as a function relates to the particle geometry and temperature. Style and Peppin (Style and Peppin 2012) defined the boundary condition at a growing ice lens:

$$\xi(t) = -\mathbf{z} \cdot \frac{1}{A_1} \int_{A_2} g(x, t)\mathbf{n}dA \tag{5}$$

Then Eq. (4) is rewritten as a kinetic formula for the equivalent water pressure:

$$P - P_n = -V\xi(t) \tag{6}$$

Employing Darcy's law, the water flow velocity under the equivalent water pressure with a distance H can be

defined as: $V = -kP_n/\mu H$; and by the combination of using Eq. (6), the water flow velocity can be defined as follows:

$$V = -k\frac{(t_a v_w P_e + Lt)}{t_a v_w (\mu H + k\xi(t))} \quad (7)$$

where k is the hydraulic conductivity, μ is the dynamic viscosity; from the numerator of Eq. (7), we find that $V = 0$ when $P_e = P_{max} = -Lt/t_a v_w$, where P_{max} is referred to as the *maximum heaving pressure*. After calculation, it is found that P_{max} is approximately 1.2 atm (0.12Mpa) when the ice lens temperature boundary is $-0.1\,^{\circ}$C. The ice lens will continue to grow ($V > 0$) if the overburden pressure is less than P_{max}.

When the FHIP in test #10 peaked at the *maximum heaving pressure*, the ice probably cannot support loads that are greater than P_{max}, causing the ice lens to melt rather than grow (Fig. 7a). Thereafter the FHIP was affected, which led to a slight decrease in the FHIP. Subsequently, the growth of the ice lens continued after the relaxation of the FHIP at the soil–restraint boundary, and the FHIP increased by a small degree. Accordingly, the FHIP experienced decrease and increase cycles, and a fluctuation existed in the FHIP with the elapsed time.

Variation of the temperature in soil column

The FHIP is the response of restraint to frost heave and is mainly induced by water flow under the thermal gradient (section "Water migration and distribution in freezing soil" above). Accordingly, it is also important to access the temperature distribution within the soil column. Freezing soil under a restrained stiffness of 11.06 kPa/mm (constant cold end temperature of $-20\,^{\circ}$C) was chosen as a representative to demonstrate the variations of the temperatures within the soil column.
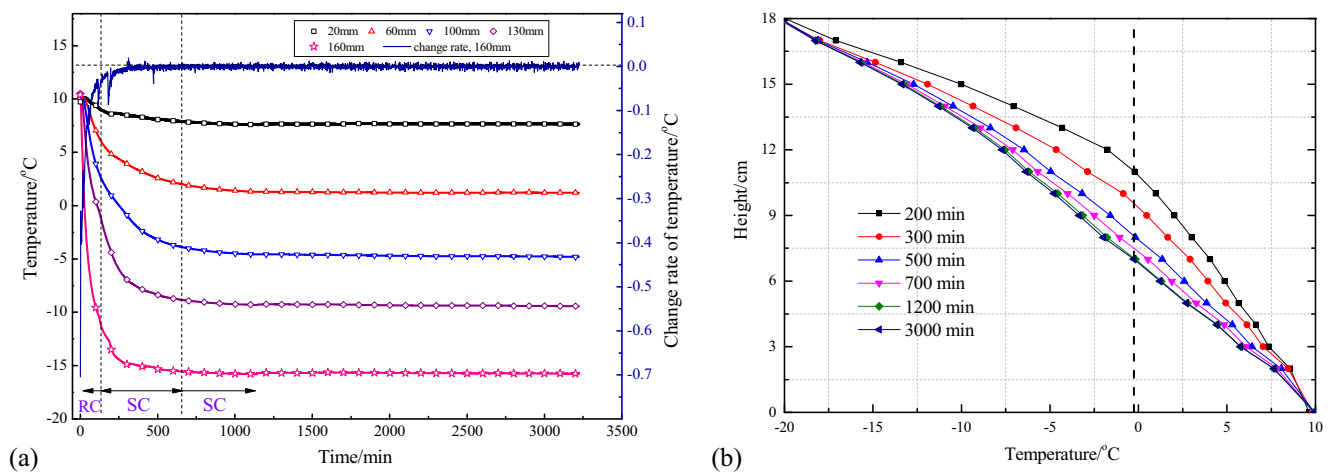
The observed transient temperature at different heights of the soil column (20mm, 60mm, 100mm, 130mm, 160mm) can be distinguished into three stages according to the evolution of the temperature change rate during freezing (Fig. 8a), i.e., *rapid cooling stage* (RC), *slow cooling stage* (SC) and *stable stage* (SS).

In the RC stage, the temperature varied rapidly from the initial value (10 $^{\circ}$C) to a lower temperature. In the SC stage, the rate of change of temperature decreased in comparison with the RC stage. Finally, after approximately 600 minutes, the temperature stabilized. From the discussion of the FHIP outlined in the section "The FHIP and maximum FHIP during freezing" above, it can be concluded that a lag exists between temperature stabilization and subsequently FHIP stabilization. Additionally, the closer the distance from the cold end, the faster the temperature dropped to the stable condition as shown in the SC stage (Fig. 8a).

Furthermore, the parameter of rate of change of temperature is characterized as a variable to represent the test conditions in the frozen zone. The rate of change of temperature can be determined as the product of the temperature gradient in the frozen zone and frost penetration rate. Mathematically, this is written as:

$$\frac{\mathrm{d}T}{\mathrm{d}t} = \frac{\mathrm{d}T}{\mathrm{d}D}\frac{\mathrm{d}D}{\mathrm{d}t} \quad (8)$$

It is obvious that the characterized variable comprises both geometrical and thermal conditions of the freezing soil. In the early stage of freezing, a dramatic change of the thermal conditions were imposed on the soil column as a result of the high temperature gradient (17.50 $^{\circ}$C/cm) and the high frost penetration rate (-0.27 cm/min).

Fig. 8 Temperature profile during transient freezing from test #7: **a** variations of test temperatures at different heights of soil column; **b** the distribution of temperature at different time

The temperature distribution changed rapidly in the early stage of freezing; the temperature change rate then decreased from a high value to a value near zero when dD/dt approached zero (Fig. 8b), i.e., when the frost front kept stationary. The vertical dashed line in Fig. 8b approximately represent the segregation temperature of the ice lens. As described in the section "Water migration and distribution in freezing soil" above, the soil can be distinguished into two zones according to the segregation temperature. The observed temperature (Fig. 8b) appears to be a bilinear distribution along the soil column, with the lower gradient in the unfrozen zone compared to the frozen zone. This is because of the existence of pore ice in the soil, thus causing the variation of the thermal parameter in different zones.

The different FHIP under various restraints

The mechanism analysis of the difference in the FHIP under various different restraints

The FHIP is induced by frost heaving under the restraint. The difference in water flow velocity results in the variation in frost heave. Therefore, in this paper the authors study the FHIP under various different restraints in an attempt to determine the difference in the FHIP, and to explore the characterized behavior of the FHIP from the view of water flow velocity. A schematic of the freezing soil under rigid restraint is shown in Fig. 9. The frozen fringe in Fig. 9 is simplified as one part of the frozen zone during the mechanical analysis.

There is no appearance of heave when the freezing soil is under the rigid restraint. The segregation pressure df induced by the growth of the ice lens dh results in the compression deformation of both the frozen and unfrozen soil. A brief identifier of the relationship between the incremental of the segregation ice thickness and the incremental of the segregation pressure can be written according to the compatibility of deformation:

$$dh = \frac{df}{E_1(\tau)}D(\tau) + \frac{df}{E_2}(L - D(\tau)) \tag{9}$$

where $E_1(\tau)$ is the elastic modulus of the frozen soil, and is a function of time τ; E_2 denotes the elastic modulus of the unfrozen soil; $D(\tau)$ represents the frost depth, and it is also a function of time; L is the height of the soil column.

Therefore, the relationship between the increment of segregation pressure and the incremental of segregation ice thickness can be determined as:

$$df = \frac{E_1(\tau)E_2}{E_1(\tau)(L - D(\tau)) + E_2D(\tau)}dh \tag{10}$$

It is assumed that the development of frost depth satisfies the following relationship:

$$D(\tau) = D_m\sin\frac{\pi}{2A}\tau \tag{11}$$

where D_m is the maximum frost depth, and A stands for the total duration time of freezing.

The deformation dh induced by the formation of ice lens acts on both frozen and unfrozen soil, resulting in the formation of the segregation pressure. Based on the theoretical calculations and experimental tests for pile foundations, Xu et al. (Xu et al. 2001) indicated that the ultimate frost heave equals the disparity between free frost heave and restrained frost heave (the direction of deformation is opposite to frost heave). The free frost heave can be divided into two parts: (i) frost heave, which is observed under the restrained condition, and (ii) the part inhibited by restraint, which causes compression of the freezing soil. Accordingly, it is considered that the FHIP f_r under rigid restraint correlates to free frost heave, since no heave appears during freezing because of the inhibiting effect
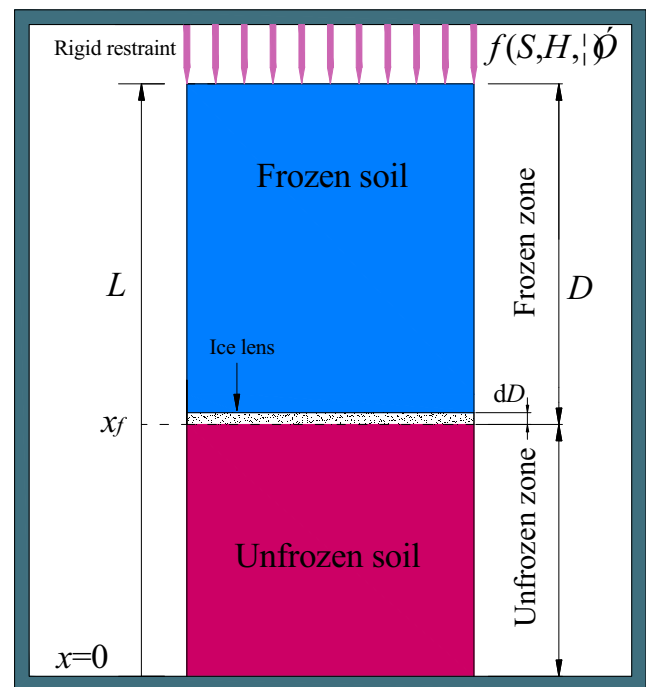

Fig. 9 Schematic of the freezing soil under rigid restraint

thereof. Therefore, the change of the FHIP f_r per unit time can be written as:

$$\frac{\mathrm{d}f_r}{\mathrm{d}\tau} = \frac{E_1(\tau)E_2}{E_1(\tau)(L-D(\tau)) + E_2D(\tau)} \frac{\mathrm{d}h}{\mathrm{d}\tau} \qquad (12)$$

where $\mathrm{d}h/\mathrm{d}\tau$ represents the rate of free frost heaving velocity.

According to the study from Hendry et al. (Hendry et al. 2016) and the laboratory tests in this study, the heaving velocity can be approximately described by an exponential function, shown in Eq. (13). Fig. 10 demonstrates the relationship between the heaving velocity and time in this study.

$$V = V_{\max}\mathrm{e}^{\frac{-\tau}{b}} \qquad (13)$$

where $V_{\max}$ is the maximum heaving rate, b is the soil parameter.

The free frost heave can be determined by integrating the heaving rate V_0 over the testing time A after freezing, the soil parameter b can then be calculated, and the heaving rate can be rewritten as:

$$V_0 = V_0^{\max}\mathrm{e}^{\frac{-\tau V_0^{\max}}{H_0}} \qquad (14)$$

Consequently, the change rate of f_r under the rigid restraint can be determined as:

$$\frac{\mathrm{d}f_r}{\mathrm{d}\tau} = \frac{E_1(\tau)E_2}{E_1(\tau)(L-D(\tau)) + E_2D(\tau)} V_0^{\max}\mathrm{e}^{\frac{-\tau V_0^{\max}}{H_0}} \qquad (15)$$

Furthermore, when the frost heave is tested under the restrained stiffness of K_1, the free heaving velocity can be divided into two parts. Part of the heaving velocity shown in Fig. 11
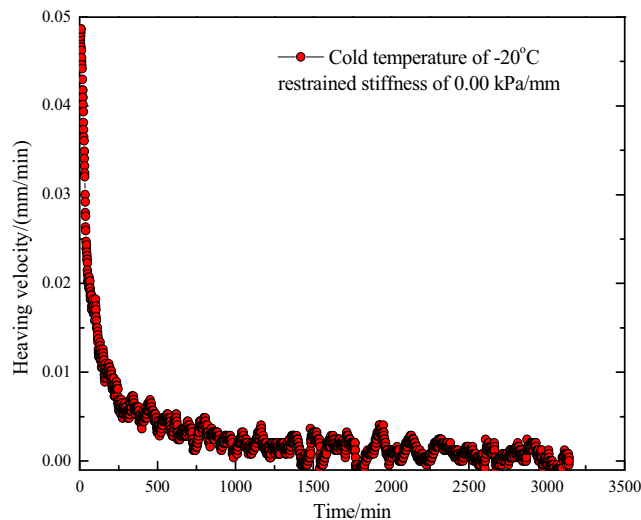

Fig. 10 Results of the heaving velocity under the free boundary associated with a constant cold end temperature of –20 °C
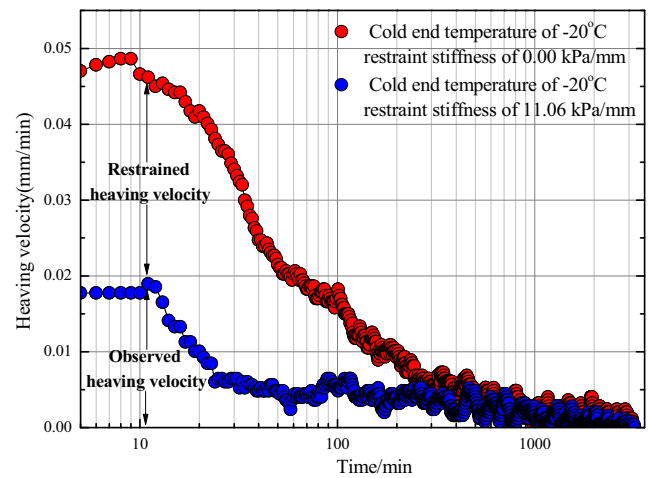

Fig. 11 The schematic of heaving velocity under the free boundary and restrained boundary

under the restrained stiffness K_1 is called the observed heaving velocity V_{K_1}, which contributes to the observed frost heave. The disparity between the free heaving velocity and the observed heaving velocity is inhibited by the restraint, which contributes the formation of the FHIP under the restrained stiffness of K_1. In addition, previous studies have found that the applied pressure has little effect on the frost penetration (Xia 2005). Therefore, the FHIP under the restrained stiffness of K_1 can be determined as the following equation shown as Eq. (16).

$$\frac{\mathrm{d}f_{K_1}}{\mathrm{d}\tau} = \frac{E_1(\tau)E_2}{E_1(\tau)(L-D(\tau)) + E_2D(\tau)} \left(V_0^{\max}\mathrm{e}^{\frac{-\tau V_0^{\max}}{H_0}} - V_{K_1}^{\max}\mathrm{e}^{\frac{-\tau V_{K_1}^{\max}}{H_1}} \right) \qquad (16)$$

where H_1 is the observed frost heave under the restrained stiffness of K_1.

From Eq. (16), it can be found that the disparity between the free heaving velocity and the observed heaving velocity results in the formation of the FHIP under the restraint. With an increase of the restrained stiffness, the observed heaving velocity decreases. This implies that the restrained heaving velocity increases, as compared to the free heaving velocity. Furthermore, the restrained heaving velocity is believed to contribute to the quantity of compression deformation of the freezing soil, which results in the increase of the FHIP. As already mentioned, the greater the restrained stiffness is, the greater the FHIP appears during the freezing.

Based on the experimental results in Table 2, a dropping behavior of the FHIP is observed with the increase of the frost heave ratio (Fig. 12). Importantly, although observed frost heave decreases with restraint, the restrained frost heave and the FHIP increases with restraint. Therefore, it is suggested for consideration when the restrained structure is applied to reduce frost heave in practical engineering,
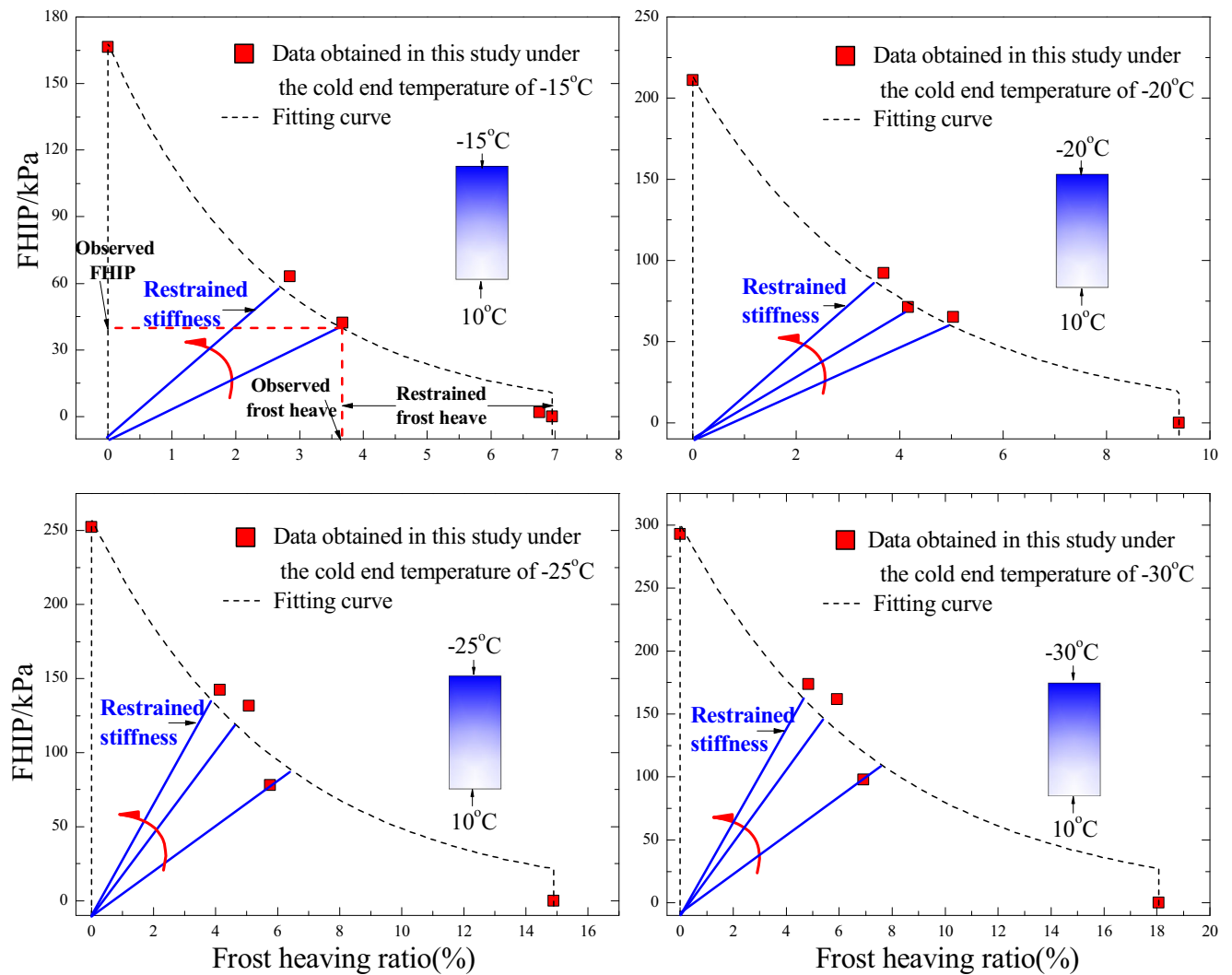
Fig. 12 Relationships between the FHIP and the frost heaving ratio under various different cold end temperatures

since the increased FHIP acting on the engineering structure is directly responsible for flaking and cracking in the supported structure.

Conclusions

A thermal gradient is a necessary condition for water flow and frost heave, since pore water solidifies into ice and thus causes suction (negative pore water pressure) at the base of the ice lens. The suction not only provides a driving force for capillary water flow, but also results in unsaturated phenomena in the unfrozen zone.

Frost heave decreases with restraint. This is because it becomes more difficult for the ice lens to emerge with restraint, and thus it decreases the water content at the frost front. Moreover, the pore structure and flow properties of freezing soil vary, since ice crystals progressively block the flow of

water, and discontinuous ice lenses result in the oscillations in water distribution.

Contrary to the trend with frost heave, the FHIP increases with restraint, and the stable stage for the FHIP lags behind the stabilization temperature. Additionally, the increase of the FHIP will cease when the ice pressure reaches the maximum heaving pressure. A mathematics description in this paper shows that the maximum heaving pressure is a function of temperature of the ice lens.

A mathematics description of the FHIP under a given restrained stiffness would aid in the explanation of the difference in the FHIP under various different restrained stiffness values. A larger restrained stiffness value causes a greater restrained deformation, and results in an increase of the observed FHIP. It is suggested that the increased phenomenon of the FHIP should be taken into consideration when restrained structure is applied to reduce frost heave in practical engineering.

References

Bronfenbrener L, Bronfenbrener R (2010) Modeling frost heave in freezing soils. Cold Reg Sci Technol 61:43–64

Cheng GD, Li X (2003) Constructing the Qinghai–Tibet Railroad: new challenges to Chinese permafrost scientists. Proceedings of the 8th International Conference on Permafrost. A.A.BALKEMA Publishers, Tokyo, pp 131–134

Gilpin RR (1979) A model of the "liquid-like" layer between ice and a substrate with applications to wire regelation and particle migration. J Colloid Interf Sci 68(2):235–251

Gilpin RR (1980) A model for the prediction of ice lensing and frost heave in soils. Water Resour Res 16(5):918–930

Harlan RL (1973) Analysis of coupled heat–fluid transport in partially frozen soil. Water Resour Res 9(5):1314–1323

Hopke SW (1980) A model for frost heave including overburden. Cold Reg Sci Technol 3(2):111–127

Hendry MT, Onwude LU, Sego DC (2016) A laboratory investigation of the frost heave susceptibility of fine-grained soil generated from the abrasion of a diorite aggregate. Cold Reg Sci Technol 123:91–98

Ji YK, Zhou GQ, Zhou Y, Matthew RH, Zhao XD, Mo PQ (2018) A separate-ice based solution for frost heaving-induced pressure during coupled thermal-hydro-mechanical processes in freezing soils. Cold Reg Sci Technol 147:22–33

Konrad JM, Morgenstern NR (1982) Effects of applied pressure on freezing soils. Can Geotech J 19(4):494–505

Konrad JM (1994) 16th Canadian Geotechnical Colloquium—frost heave in soils—concepts and engineering. Can Geotech J 31(2):223–245

Lai YM, Wu H, Wu ZW, Liu SY, Den XJ (2000) Analytical viscoelastic solution for frost force in cold-region tunnels. Cold Reg Sci Technol 31(3):227–234

Lai YM, Pei WS, Zhang MY, Zhou JZ (2014) Study on theory model of hydro-thermal–mechanical interaction process in saturated freezing silty soil. Int J Heat Mass Tran 78:805–819

Ma MY, Cheng Y (2007) Development and prospects of research on freezing pressure of frozen shaft in deep thick alluvium. Journal of Anhui Institute of Architecture and Industry 15(5):8–12 (in Chinese)

Nixon JF (1991) Discrete ice lens theory for frost heave in soil. Can Geotech J 28(6):843–859

Oliphant JL, Tice AR, Nakano Y (1983) Water migration due to a temperature gradient in frozen soil. In Proceedings of the 4th International Conference on Permafrost. Fairbanks, AK, pp 951–956

O'Neill K, Miller RD (1985) Exploration of a rigid ice model of frost heave. Water Resour Res 21(3):281–296

Palmer AC, Williams PJ (2003) Frost heave and pipeline upheaval buckling. Can Geotech J 40:1033–1038

Rong CX (2006) A study on mechanical characteristic of frozen soil wall and shaft lining as well as their interaction mechanism in deep alluvium. PhD. Thesis, University of Science and Technology of China. Anhui, China (in Chinese)

Sheng DC, Axelsson K, Knutsson S (1995a) Frost heave due to ice lens formation in freezing soils: 1. Theory and verification. Hydrol Res 26(2):125–146

Sheng DC, Axelsson K, Knutsson S (1995b) Frost heave due to ice lens formation in freezing soils: 2. Field application. Hydrol Res 26(2):147–168

Style RW, Peppin SSL (2012) The kinetics of ice-lens growth in porous media. J Fluid Mech 692(2):482–498

Sheng DC, Zhang S, Yu ZW, Zhang JS (2013) Assessing frost susceptibility of soils using PCHeave. Cold Reg Sci Technol 95(11):27–38

Taylor GS, Luthin JN (1978) A model for coupled heat and moisture transfer during soil freezing. Can Geotech J 15(4):548–555

Worster MG, Wettlaufer JS (1999) The fluid mechanics of premelted liquid films. In: Shyy W, Narayanan R (Eds.) Fluid dynamics of interfaces. Cambridge University Press, Cambridge, pp 339–355.

Wang YS, Xue LB, Cheng JP, Han T, Li JH (2009) In-situ measurement and analysis of freezing pressure of vertical shaft lining in deep alluvium. Chinese Journal of Geotechnical Engineering 31(2):207–212 (in Chinese)

Wu DY, Lai YM, Zhang MY (2017) Thermo–hydro–salt–mechanical coupled model for saturated porous media based on crystallization kinetics. Cold Reg Sci Technol 133:94–107

Xu XY, Li HS, Qiu MG, Tao ZX (2001) Calculation of frost heave in seasonal frozen soil under piled foundation restrain condition. Journal of Harbin University of C. E. & Architecture 34(6):8–11 (in Chinese)

Xia DJ (2005) Frost heave (Ph.D. Thesis), University of Alberta, Alberta, Canada.

Zhou Y, Zhou GQ (2012) Intermittent freezing mode to reduce frost heave in freezing soils—experiments and mechanism analysis. Can Geotech J 49(6):686–693

Zhang S, Teng J, He Z, Liu Y, Liang S, Yao Y, Sheng D (2016) Canopy effect caused by vapour transfer in covered freezing soils. Geotechnique 66(11):927–940

Zhang XY, Zhang MY, Lu JG, Pei WS, Yan ZR (2017) Effect of hydro-thermal behavior on the frost heave of a saturated silty clay under different applied pressures. Appl Therm Eng 117:462–467